infrastructures

MDPI

Article

Response Surface Methodology Approach for the Prediction and Optimization of the Mechanical Properties of Sustainable Laterized Concrete Incorporating Eco-Friendly Calcium Carbide Waste

Auwal Ahmad Khalid [1], Abdurra'uf. M. Gora [1,*], A. D. Rafindadi [1], Sadi I. Haruna [2,*] and Yasser E. Ibrahim [2]

[1] Department of Civil Engineering, Faculty of Engineering, Bayero University Kano, Kano P.M.B 3011, Nigeria; auwaldarki@gmail.com (A.A.K.); adrafindadi.civ@buk.edu.ng (A.D.R.)
[2] Engineering Management Department, College of Engineering, Prince Sultan University, Riyadh 11586, Saudi Arabia; ymansour@psu.edu.sa
* Correspondence: amgora.civ@buk.edu.ng (A.M.G.); sharuna@psu.edu.sa (S.I.H.)

Abstract: This study investigated the combined effects of calcium carbide waste (CCW) and lateritic soil (LS) on sustainable concrete's fresh and mechanical properties as a construction material for infrastructure development. The study will explore the possibility of using easily accessible materials, such as lateritic soils and calcium carbide waste. Therefore, laterite soil was used to replace some portions of fine aggregate at 0% to 40% (interval of 10%) by weight, while CCW substituted the cement content at 0%, 5%, 10%, 15%, and 20% by weight. A response surface methodology/central composite design (RSM/CCD) tool was applied to design and develop statistical models for predicting and optimizing the properties of the sustainable concrete. The LS and CCW were input variables, and compressive strength and splitting tensile properties are response variables. The results indicated that the combined effects of CCW and LS improve workability by 18.2% compared to the control mixture. Regarding the mechanical properties, the synergic effects of CCW as a cementitious material and LS as a fine aggregate have improved the concrete's compressive and splitting tensile strengths. The contribution of LS is more pronounced than that of CCW. The established models have successfully predicted the mechanical behavior and fresh properties of sustainable concrete utilizing LS and CCW as the independent variables with high accuracy. The optimized responses can be achieved with 15% CCW and 10% lateritic soil as a substitute for fine aggregate weight. These optimization outcomes produced the most robust possible results, with a desirability of 81.3%.

Keywords: sustainable concrete; calcium carbide waste; laterite soil; mechanical properties; response surface methodology

Citation: Khalid, A.A.; Gora, A.M.; Rafindadi, A.D.; Haruna, S.I.; Ibrahim, Y.E. Response Surface Methodology Approach for the Prediction and Optimization of the Mechanical Properties of Sustainable Laterized Concrete Incorporating Eco-Friendly Calcium Carbide Waste. *Infrastructures* **2024**, *9*, 206. https://doi.org/10.3390/infrastructures9110206

Academic Editors: Yangyang Li and Zhuo Chen

Received: 13 October 2024
Revised: 14 November 2024
Accepted: 15 November 2024
Published: 17 November 2024

1. Introduction

The construction industry is currently struggling to incorporate sustainability into its production processes. This includes pursuing new, environmentally friendly raw materials and products that can help mitigate carbon dioxide emissions [1]. One viable approach is the reuse of industrial and agricultural waste to create sustainable building materials, which can also contribute to reducing CO_2 emissions, reducing sand extraction, and conserving natural resources [2–4]. Research trends in material development are increasingly focused on finding alternatives due to the high costs associated with traditional materials and the difficulties securing funding for construction projects. Some other options include using pozzolana as a cement substitute or incorporating various agricultural waste products and industrial by-products as additives or mixtures [3,5,6]. In countries with limited resources, substituting readily accessible materials for typical aggregates in concrete for structural purposes might be cost-effective, given the establishment of a reliable design database on concrete made with these materials [7].

Laterite, a naturally occurring soil found extensively throughout the tropics and subtropics, is one of these minerals. This material has served as a base course for building highways and a filling material for foundations with promising results [7,8]. Research efforts have focused on using laterite as the primary aggregate in producing what are known as lateritic blocks, which are building blocks. Using this easily accessible and affordable material in concrete construction in areas with abundant deposits has the potential to drastically lower concrete costs [2,9], and there are various studies on the impact of laterite inclusion on the material's mechanical and serviceability characteristics and durability [10–12]. Udoeyo et al. [7] investigated the properties of concrete when laterite is used in place of sand in either partial or total replacement. Their findings indicated that the amount of laterite added to the concrete improved its workability and reduced mechanical properties. However, they reported that compressive strength can reach up to 20 MPa when the laterite soil is limited to 40% replacement. Ettu et al. [13] investigated the suitability of employing laterite as the only fine aggregate in structural concrete production. The result indicated that laterized concrete satisfied the minimum 25 MPa compressive strength requirement for reinforced concrete. Raja et al. [14] produced high-strength concrete (HSC) samples of M60 grade by substituting the manufactured sand with laterite at 25, 50, 75, and 100 percent by weight to obtain suitable mixes to investigate its mechanical properties and microstructural analysis. Moreover, 10% micro silica and 10% of fly ash (FA) were incorporated into mixes. It was reported that the optimum mix was achieved with 25% laterite replacement. The bending behavior of laterized beams is 11.3% higher than reference samples. Ukpata et al. [15] investigated the effects of varying aggregate sizes (12 mm, 20 mm, and 40 mm) on the strength of concrete substituted with 10% and 25% laterite for fine aggregate. The result showed that the mechanical properties of concrete were affected when laterite was used to replace fine aggregate; an increase in laterite percentage led to a decrease in mechanical properties. However, 0% and 10% laterite substitution achieve the required strength.

A byproduct of the process of producing acetylene gas (C_2H_2) is calcium carbide waste (CCW). The main uses of acetylene gas are welding, agricultural fruit ripening, metal cutting, and space heating. A chemical reaction between calcium carbide and water yields CCW, as demonstrated by Equation (1).

$$\boldsymbol{CaC_2 + 2H_2O \rightarrow\ C_2H_2 + Ca(OH)_2} \quad (1)$$

Calcium carbide waste is characterized by a high alkalinity (pH > 12) and consists of approximately 92% calcium hydroxide ($Ca(OH)_2$) by mass [1,16]. The CCW is a byproduct of manufacturing compounds and building materials. The residual construction wastes are stockpiles, which occupy land and contaminate water resources and the adjacent environment [17,18]. When combined with other pozzolanic materials containing siliceous and aluminous compounds in cementitious mixtures, $Ca(OH)_2$ reacts with silicon oxide or silicon and aluminum oxides in the pozzolans. This reaction leads to additional calcium silicate hydrates (C-S-H), which contribute to concrete strength development [3,19]. Furthermore, increasing amounts of calcium carbide in cement mortar yields favorable workability, setting time, and flexural and compressive strength results. However, it was also observed that water absorption increased as the proportion of CCW rose [20]. Obeng et al. [21] investigated the feasibility of using calcium carbide residue (CCR) in metakaolin-based geopolymer mortars with regard to their sulfate resistance. The results showed that when compared to the geopolymer without CCR, the addition of CCR increased compressive strength by 26.12%. The geopolymer material with CCR exhibited a decreased sulfate resistance compared to those without CCR. Adamu et al. [5] examined the water absorption, permeability, and hardened characteristics of pervious concrete modified with hybridized rice husk ash (RHA) and CCW. The authors reported that both RHA and CCW negatively affected the durability of Portland cement. Khongpermgoson et al. [22] studied the effect of ground coal bottom ash (GBC) and CCR on concrete's compressive strength and durability-related properties. The authors reported that the concrete made from GBC only

showed increased compressive strength. The microstructure and residual performance of self-compacting concrete incorporated with copper slag waste after high-temperature exposure has been evaluated [23]. Gao et al. [24] investigated the stress–strain relationship of low-carbon concrete stimulated with CCR subjected to uniaxial and triaxial stresses. Chen et al. [25] developed CCR alkali-activated cement-based materials containing waste glass powder to study the rheological and hardened properties. The authors reported that the replacement of fly ash with glass powder facilitates the alkali-activated reaction at some point. Jaramillo et al. [26] developed non-structural concrete elements from construction and demolition waste (CDW) for sustainable building infrastructures. The authors utilize recycled microplastic (RMP) and CDW for various contents. They showed that concrete elements made from recyclable waste materials revealed an increase in acoustic and thermal insulation behavior.

RSM is a robust methodology and a set of statistical techniques that are helpful for modeling and problem analysis when optimizing a response influenced by several variables [27,28]. Statistical modeling, material property prediction, and optimization are the main applications for the multivariable regression analysis approach. RSM is more appropriate for building and construction applications, particularly when multiple variables are involved. The RSM technique aims to investigate the influence of one or more input features on a response or behavior with fewer experiments, which will save time and resources. It can also develop model equations to estimate the examined properties with the most significant number of variables by optimizing the proportions of the variables that will produce the best results [29–31]. Over the decades, research has been conducted to formulate models, experiment design, and optimize the properties [32–34]. Siamardi et al. [35] experimented with and developed RSM models for estimating the characteristics of lightweight self-compacting concrete superplasticizers and light-expanded clay as the input variables. The concrete properties incorporating steel fiber and limestone powder were estimated and optimized by Awolusi et al. [29] using the RSM model. Haruna et al. [32] developed an RSM/CCD model for optimizing the impact resistance of fiber-reinforced concrete modified with nanomaterials. Haque et al. [36] estimated and optimized the characteristics of concrete containing rice husk ash and glass fiber. A previous study [31] reported that the workability of the concrete is reduced by adding laterite to the concrete matrix. Therefore, an appropriate laterized concrete mixture is required to achieve workable, eco-friendly concrete. To promote sustainable construction materials and minimize waste, this study investigates the synergic effects of lateritic soil and calcium carbide waste on the fresh and mechanical properties of the concrete. Using central composite design, the RSM technique was applied to estimate and optimize the laterite concrete mixtures. The developed statistical models were validated for the mechanical properties. The findings in this study could offer valuable insight into using CCW in laterite concrete mixtures for structural applications.

2. Materials and Methods

2.1. Materials

The laterite concrete was prepared using ordinary Portland cement (Grade 42.5R) and complied with ASTM C150-00 [37]. The chemical properties of the cement are summarized in Table 1. The concrete constituents include cement, CCW, LS, fine aggregate, and coarse aggregate. The clean river sand was used as the fine aggregate with a large sieve size of 4.75 mm. The sand has a fineness modulus of 2.82 and an apparent density of 2626 kg/m^3. The coarse aggregate was crushed granite with a nominal particle size of 20 mm with a specific gravity of 2.69, a water absorption rate of 1.68%, and a bulk density of 1572 kg/m^3.

The CCW was sourced from a commercial mechanical welding workshop. The Sample CCW sample was treated at a high temperature (110 °C) to remove the moisture content and then ground into a powder and sieved using a 75 µm sieve to obtain the desired particle size retention. It has a lower specific gravity of 2.34. The chemical composition of CCW is also portrayed in Table 1. The laterite soil used in this study is uniformly graded with a

C_u of 9.48 (i.e., $C_u < 40$) with liquids and plastics limits of 40.91% and 30.67%, respectively, and a plasticity index (PI) of 10.23%. The specific gravity of the LS is 2.54, and the natural moisture content is 11.52%. The particle size gradation aggregate materials were obtained following BS 882 [33], and the gradation curve is depicted in Figure 1.

Table 1. Chemical composition of cementitious materials.

Oxides	Chemical Composition (%)	
	OPC	CCW
SiO_2	20.76	3.76
Al_2O_3	5.54	1.46
Fe_2O_3	3.35	0.12
CaO	61.4	92.77
MgO	2.46	1.25
K_2O	0.76	-
Na_2O	0.19	-
SrO	-	0.87
Nb_2O_5	-	0.11
SO_2	-	0.75
TiO_2	-	0.04
BaO	-	1.00
Sb_2O_3	-	1.00
Loss of Ignition	2.24	-

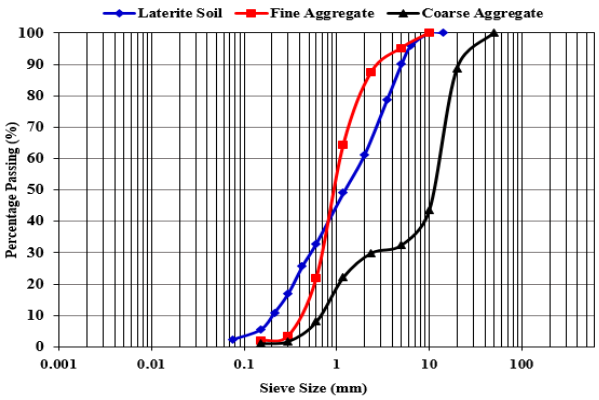

Figure 1. Grading curves of aggregate materials.

2.2. Specimen Preparation

The concrete mixture was prepared following the mixing procedure specified in BS 1881, P 125 [38]. The concrete mixtures were produced by replacing fine aggregate with LS at 0, 10%, 20%, 30%, and 40%, and CCW was added at 0%, 5%, 10%, 15%, and 20% by weight of cement. The process starts with a dry mixing of constituent materials such as fine and coarse aggregate, LS, CCW, and cement for 2 min. Then, water was added to the dried mix and continued mixing for another 4 min until a homogeneous mixture was achieved. The freshly prepared laterite concrete was cast into the molds for compressive and splitting tensile strength tests. Before specimen casting, the molds were cleaned and oil-lubricated. The cast specimens were removed from the molds after 24 h and placed in a standard curing room (T = 20 ± 2 °C, RH ≥ 98%) until the specified ages of 7, 24, and 28 days.

2.3. Mix Proportioning of Concrete Using RSM

RSM analysis was used to establish appropriate portions of cement, laterite soil, waste calcium carbide, coarse aggregate, fine aggregate, and water to obtain the desirable workability and mechanical properties. The w/c ratio of 0.55 was used to prepare laterized concrete mixes in this study, and the concrete's mix proportion was formulated using the

principles specified in the building research establishment (BRE) [39] mix design method (formerly known as the DOE method). In this study, RSM analysis was performed using Design Expert version 13. To develop a statistical model of laterite concrete modified with CCW, a central composite design with α ranging from −1.41 to 1.41 was used, with CCW and laterite soil serving as independent variables. Five (5) levels correspond to each parameter: 0% to 20% CCW in place of cement. Likewise, the percentages of fine aggregate content substituted in laterite soils are 0%, 10%, 20%, 30%, and 40%, respectively. Table 2 shows the mix proportion of the concrete materials used to prepare the laterite concrete, and the 13 mixes generated by the RSM software (https://rsmus.com/services/digital-transformation/enterprise-resource-planning.html accessed on 14 November 2024) using various combinations of factors are summarized in Table 3. There are eight (8) axial points and five (5) center points in the thirteen (13) mixes. The center points are mixed combinations that are repeated. The repeated mixes, also known as duplicated design points, are used to determine the model's lack of fit. The "Lack of Fit Tests" chart contrasts the "Pure Error" from duplicated design points with the residual error. The model should not be utilized as a response predictor if there is a significant lack of fit, as shown by a low probability value ("Prob > F").

Table 2. Mix proportioning using RSM.

Std	Run	Coded Values		Actual Values	
		CCW (%)	Lateritic Soil (%)	CCW (%)	LS (%)
5	1	−1.41421	0	0	20
13	2	0	0	10	20
1	3	−1	−1	5	10
9	4	0	0	10	20
7	5	0	−1.41421	10	0
10	6	0	0	10	20
11	7	0	0	10	20
12	8	0	0	10	20
2	9	1	−1	15	10
4	10	1	1	15	30
6	11	1.41421	0	20	20
8	12	0	1.41421	10	40
3	13	−1	1	5	30

Table 3. The mix proportion of concrete materials based on RSM analysis/kg/m^3.

Mix ID	Cement	Sand	Coarse Aggregate	Water	CCW	LS
M1(5C10L)	327.75	423	1495	190	17.25	47
M2(15C10L)	293.25	423	1495	190	51.75	47
M3(5C30L)	327.75	329	1495	190	17.25	141
M4(15C30L)	293.25	329	1495	190	51.75	141
M5(0C20L)	345.00	376	1495	190	0	94
M6(20C20L)	276.00	376	1495	190	69	94
M7(10C0L)	310.50	470	1495	190	34.5	0
M8(10C40L)	310.50	282	1495	190	34.5	188
M9(10C20L)	310.50	376	1495	190	34.5	94
M10(10C20L)	310.50	376	1495	190	34.5	94
M11(10C20L)	310.50	376	1495	190	34.5	94
M12(10C20L)	310.50	376	1495	190	34.5	94
M13(10C20L)	310.50	376	1495	190	34.5	94
M14(0C0L)	345.00	470	1495	190	0	0

2.4. Testing Methods

2.4.1. Slump Test

The workability of the freshly prepared laterite concrete was determined using a slump test following the procedure described in British standards [40]. For each mix, a steel slump cone filled in three layers with fresh concrete was used to measure the slump of the laterite concrete. After compaction, the cone was gently taken off, and the height difference between the cone's top and freshly mixed concrete was measured and recorded, as shown in Figure 2.

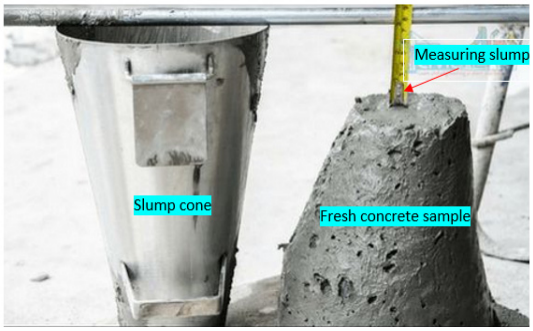

Figure 2. Slump flow test setup.

2.4.2. Mechanical Properties Test

The hardened properties test of the laterite concrete was performed using the universal testing machine, following British standards [41], as shown in Figure 3a,b for compressive and splitting tensile tests, respectively. The compressive strength of the laterized concrete was using cube specimens with dimensions of 100 mm × 100 mm × 100 mm, and splitting tensile strength was obtained using cylindrical specimens measuring 100 mm × 200 mm. For every laterite concrete mix, nine (9) specimens (three specimens on each testing date) were produced and tested after 7, 14, and 28 days of curing, and the mean result was recorded as strength value at the particular testing date. The compressive and splitting tensile strength of laterite concrete can be determined using Equations (2) and (3).

$$f_c' = \frac{P_c}{A} \tag{2}$$

$$T_{avg} = \frac{2P_{cy}}{\pi LD} \tag{3}$$

where A is the cube's cross-sectional area (mm^2), P is the applied test load on cubes (kN), P_{cy} is the applied test load on cylinders (kN), D is its diameter of concrete cylinders (mm), and L is the cylinder specimen's length (mm).

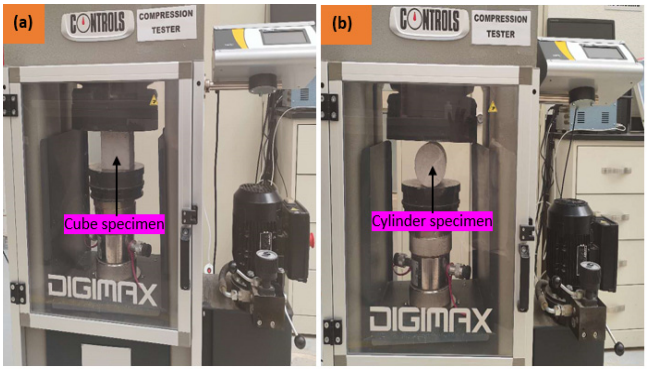

Figure 3. Experimental setup for (**a**) compressive and (**b**) splitting tensile test.

2.5. Response Surface Methodology

RSM is the best tool for establishing the mathematical relationship between input parameters and output variables [28]. It has enhanced usefulness in situations where examining the impact of several parameters on one or more output variables is necessary to reduce the number of trials needed. It can also be used to establish principles for each independent variable to optimize some of the results. A further crucial component of RSM analysis is the adequate interpretation of the experiments for the non-linear surface of the experimental data [42,43]. The variables and responses in RSM models may take the form of linear mathematical relationships, as shown in Equation (4). However, since curvature is typically present in the data, linear models that relate the responses to the input variables are inappropriate. The most appropriate polynomial model type in this situation is one with greater degrees, as indicated by the second order function in Equations (4) and (5) [28,30,42,44]

$$\eta = \beta_0 + \beta_1\chi_1 + \beta_2\chi_2 + \cdots + \beta_k\chi_k + \varepsilon \quad (4)$$

$$\eta = \beta_0 + \sum_{j=1}^{k}\beta_j\chi_j + \sum_{j=1}^{k}\beta_{jj}\chi_j^2 + \sum_{i<}\sum_{j=2}^{k}\beta_{ij}\chi_i\chi_j + \varepsilon \quad (5)$$

where η represents the expected outcome (response model); β_0 denotes the intercept or regression coefficients; β_1 and β_2 denote the first and second variable coefficients, respectively; and χ_1 and χ_2 are the first and second independent variables; β_i, β_{jj}, and β_{ij} denote the linear, quadratic, and interaction coefficients; χ_i and χ_j represent the linear and quadratic coded values for the variables, respectively; and E and n represent the residual error and number of variables.

The mathematical expression relating the input and outcome parameters can be developed utilizing various model types, including historical, one-factor, Box-Behnken, Central Composite (CCD), etc. The choice of each model type relied on the quantity and degree of variability of the independent variables. However, the CCD approach is the most efficient and broadly utilized. This is due to its ability to estimate model responses using fewer experimental findings while capturing every variable within the predetermined ranges. The CCD model allows for the choice of α (the distance measured from the design center to the axial run); the value of α is contingent upon the total points within the factorial design section [45]. Each variable in CCD is adjusted at five different levels: $+\alpha$, $-\alpha$, midpoints (central-level), and axial/factorial points $(-1, +1)$ [28,36,43]. Therefore, CCD was employed in this study to predict and optimize the responses. The figure shows the CCD framework, according to four points revealing the factorial points (± 1) and 4 central points clarifying ($\pm\alpha$) design points (see Figure 4).

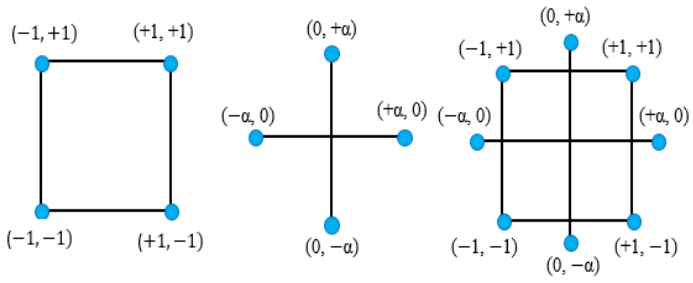

Figure 4. Central composite design (CCD) frameworks.

3. Results and Discussions

3.1. Slump Test Result

Figure 5 presents the slump values of a concrete mixture containing different CCW and LS contents. From Figure 5, it can be noted that the combined effects of CCW and LS increase the workability of a concrete mixture, as reflected in Mix 3 (5C30L), Mix 4

(15C30L), Mix 6 (20C20L), and Mix 8 (10C40L), with slump values higher than that of the control mix. Conversely, Mix 5 (0C20L), which included 20% laterite soil and 0% CCW, had a slump value of 17 mm, whereas Mix 7 (10C0L), which contained 10% CCW and 0% laterite soil, had a slump value of 16 mm, which was less than the control mix's slump of 18 mm. The remarkable slump values of 22 mm were observed in Mix 4 (15C30L), and Mix 8 (10C40L) is 18.2% higher than that of the control mix. Conversely, compared to the control mix, the remaining mixes had lower slump values. The results clearly show that compared to the control concrete mix, the laterite and CCW concrete mixes exhibited a higher slump. The little increase in slump might be attributed to CCW's particle packing effect, which reduces the amount of water required for plasticization [46]. Furthermore, it was proven by [20] that the CCW particle parking effect of voids in the hydration product is perhaps the primary influencing factor.

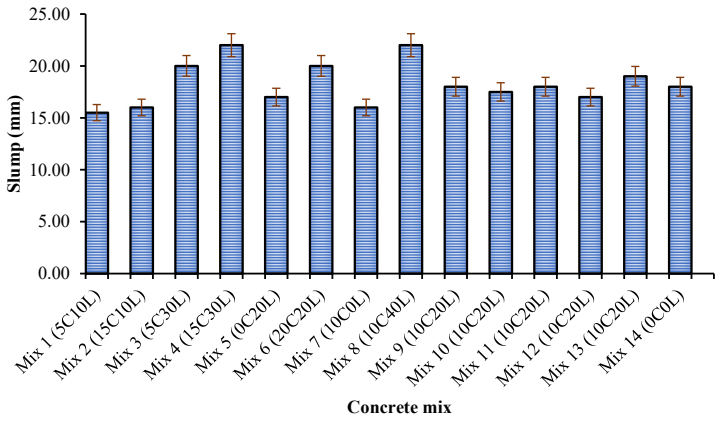

Figure 5. Slump test result of laterite concrete containing CCW.

3.2. Mechanical Properties

3.2.1. Compressive Strength

The compressive strengths of concrete containing various portions of LS and CCW tested at 7, 14, and 28 d curing ages are shown in Figure 6. The results indicated that all concrete samples experience an increase in compressive strength with age, regardless of their replacement amount. The compressive strength of the control sample (Mix 14: 0C0L) at the 7, 14, and 28 d are found to be 11.4, 16, and 20 MPa, respectively. Mix 6 concrete samples with 20% CCW and 20% laterite soil had the highest compressive strength at 7, 14, and 28 days, which were 12.0 MPa, 16.5 MPa, and 22.5 MPa, respectively. Conversely, Mix 12, which contains 10% CCW and 20%, revealed the lowest compressive strength of 9 MPa, 11.5 MPa, and 13.5 MPa at 7, 14, and 28 d of curing age, respectively. The lower strength of Mix 12 is attributed to the negative effect of LS, which had decreased compressive and lower CCW content and was unable to mitigate the loss of strength in the mix. The compressive strength was significantly increased by adding CCW. This might be explained by the pozzolanic reaction between the SiO_2 from the laterite and the $Ca(OH)_2$ from cement hydration products and CCW. This reaction produces additional C-S-H gels, the primary constituents in concrete that develop strength. This is consistent with the research done by [47]. An increased water need was also due to increased CCW and laterite soil added. This could be attributed to the mix's greater surface area and lower water content. As a result, the laterized concrete mix's particle agglomeration and insufficient uniformity decrease compressive strength [5]. A study by Ukpata et al. [15] reported a decrease in the compressive strength of concrete due to the high content of laterite soil. However, 10% laterite substitution achieves the required strength. This agreed with the finding of this study, where the compressive strength of some laterized concrete contusing CCW was lower than that of the control mix (Mix 14) at all curing ages, except for Mixes 3, 5, and 11 only at 7 days compared to the control, which may be attributed to the pozzolanic reaction at earlier ages. The low rate of pozzolanic reaction of silicon dioxide (SiO_2) and calcium

hydroxide of CCW in the mixes might cause the lowering of strength values, especially at an early age. Additionally, it can be shown from the results that the compressive strength increases when CCW replaces cement by more than 10%. As a result, laterized concrete with sufficient compressive strength appropriate for structural application is produced when CCW and laterite soil are properly balanced.

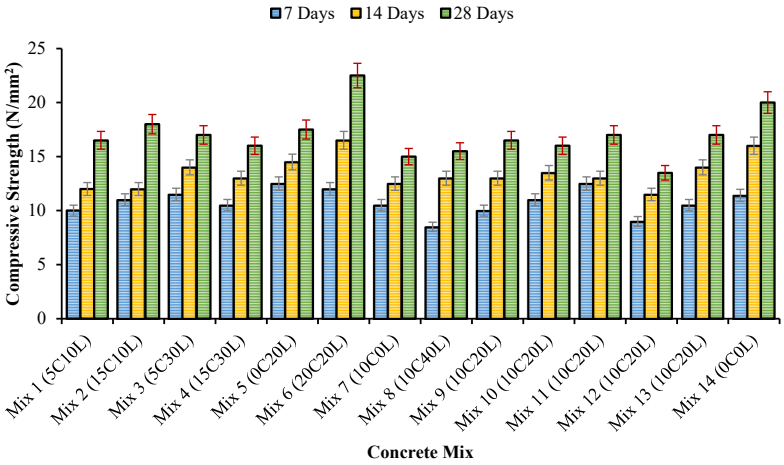

Figure 6. Compressive strength of laterite concrete modified with CCW.

3.2.2. Splitting Tensile Strength

Figure 7 shows the splitting tensile of laterite concrete modified with different CCW content tested at 7, 14, and 28 d. As seen in Figure 7, it can be noted that splitting tensile strength properties follow a similar behavior to compressive strength. The persistent cement hydration reaction during curing causes the splitting tensile strength to increase with curing age gradually. Mix 6 (20C20L) demonstrated the highest splitting tensile strength at 7, 14, and 28 days, 1.42 MPa, and 2.40 MPa, compared to other mixes. However, the tensile strength decreased in splitting tensile strength with increased LS content. This could be because of the weak link between the soil particles and the matrix of solidified concrete paste, which causes tiny cracks and a sudden loss of strength. The cement paste and aggregate bond failure consequently resulted in a reduction in the splitting tensile strength. Furthermore, this is consistent with the findings of past studies [48]. Moreover, the large surface area of CCW, which fortifies the bond between the aggregate particles and the cement matrix, causes the splitting tensile strength to decrease.

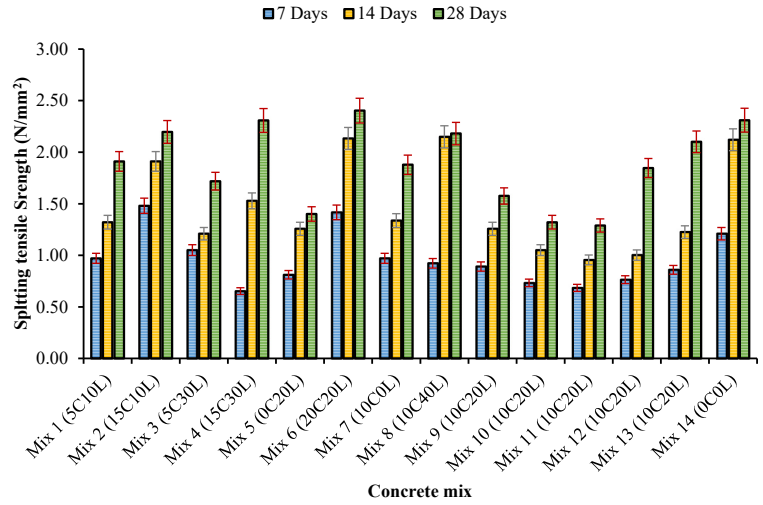

Figure 7. Splitting tensile strength of laterite concrete modified with CCW.

3.3. Statistical Analysis of Responses

3.3.1. RSM Model for Compressive Strength

The interaction between the input factors (CCW and LS) and the responses (compressive strength) was evaluated using ANOVA. The coefficient of determination (R^2) assessed the validity of the quadratic function of the CCD model, which was evaluated and validated using the probability function (*p*-value) at a 95% confidence level. The model was developed according to the coded factors. The 7, 14, and 28-day compressive strength responses were utilized to generate the prediction model. The following second-order polynomial Equations (6)–(8) represent the empirical relationship between the variables and the compressive strength:

$$F_{C-7} = 10.50 - 0.1509A - 0.1143B - 0.6250AB + 0.8750A^2 - 0.7500B^2 \quad (6)$$

$$F_{C-14} = 13.20 - 0.1509A + 0.5777B - 0.3750AB + 0.4312A^2 - 0.5687B^2 \quad (7)$$

$$F_{C-28} = 16.0 + 0.7803A + 0.0884B - 0.2500AB + 1.3300A^2 - 0.5437B^2 \quad (8)$$

where A and B stand for the corresponding percentages of the CCW and lateritic soil components, and $F_{C\text{-}7}$, $F_{C\text{-}14}$, and $F_{C\text{-}28}$ indicate the concrete's 7, 14, and 28-day compressive strengths (MPa), respectively.

It can be seen in Equations (6) to (8) the parameters and interactions considerably impacted the compressive strength. Table 4 summarizes the ANOVA result of quadratic models for estimating compressive strength at different curing ages. It can be noted that most of the model's terms revealed *p*-values less than 0.05, for instance, the terms A2, B2, and AB for the 7-day responses, which are significant. Generally, the model terms in both cases have *p*-values of less than 0.05, showing they are significant. However, the 28-day model terms showed non-significance for terms B and AB, with *p* values > 0.05. The model terms with *p*-values higher than 0.05 indicate no significant lack of fit, resulting in 40.67%, 37.63%, and 65.57% probability for noise to produce F-values of 1.24, 1.35, and 0.67 for the compressive strength for 7, 14, and 28 days, respectively.

Table 4. ANOVA result of compressive strength models.

Response	Source	Sum of Squares	Mean Square	F-Value	*p*-Value	Significance
$F_{C\text{-}7}$ (MPa)	Model	12.46	2.49	18.11	0.0007	significant
	A-CCW	0.1821	0.1821	1.32	0.2878	
	B-LS	0.1045	0.1045	0.7591	0.4125	
	AB	1.56	1.56	11.35	0.0119	
	A^2	5.33	5.33	38.70	0.0004	
	B^2	3.91	3.91	28.43	0.0011	
	Lack of Fit	0.4634	0.1545	1.24	0.4067	insignificant
$F_{C\text{-}14}$ (MPa)	Model	7.47	1.49	17.30	0.0008	significant
	A-CCW	0.1821	0.1821	2.11	0.1897	
	B-LS	2.67	2.67	30.91	0.0009	
	AB	0.5625	0.5625	6.51	0.0380	
	A^2	1.29	1.29	14.98	0.0061	
	B^2	2.25	2.25	26.06	0.0014	
	Lack of Fit	0.3045	0.1015	1.35	0.3763	insignificant
$F_{C\text{-}28}$ (MPa)	Model	21.15	4.23	12.23	0.0024	significant
	A-CCW	4.87	4.87	14.08	0.0072	
	B-LS	0.0625	0.0625	0.1806	0.6836	
	AB	0.2500	0.2500	0.7224	0.4235	
	A^2	12.33	12.33	35.63	0.0006	
	B^2	2.06	2.06	5.94	0.0449	
	Lack of Fit	0.7224	0.2408	0.5666	0.6657	not significant

where A and B indicate the percentage of CCW and lateritic soil, AB denotes the interaction effects, A^2 and B^2 represent the second-order effect, *p* values denote probability values, and F-values represent Fisher statistical test values.

Table 5 presents the performance evaluation of the compressive strength model. The coefficient of regression is the main statistical indicator to assess the performance of the developed model. The 7-day compressive strength model has the highest R^2 value, which clarifies and validates its greater significance than the other models. The difference between each model's predicted and adjusted R^2 values was lower than 0.2, indicating that the model terms substantially agreed. Moreover, a lower standard deviation indicates the model's fitness and suitability with their mean values. The adequate precision (AP) was also applied to assess the model performance. The values anticipated at the design point are compared to the average predicted error. The model's AP values for this investigation's 7, 14, and 28-day compressive strengths were 14.38, 15.19, and 12.46, respectively. As all the AP values were more than 4, the model is suitable for predicting compressive strength. The scatter plot between the predicted and observed values of compressive strength at the different curing ages is depicted in Figure 8.

Table 5. Performance indicators for compressive strength models.

Factors	$F_{C\text{-}7}$ (MPa)	$F_{C\text{-}14}$ (MPa)	$F_{C\text{-}28}$ (MPa)
Std. Dev.	0.3710	0.2939	0.5883
Mean	10.54	13.12	16.88
CoV. (%)	3.51	2.24	3.48
R^2	0.9282	0.9252	0.8973
Adjusted R^2	0.8770	0.8717	0.8239
Predicted R^2	0.6963	0.6738	0.6694
Adeq Precision	14.3831	15.1783	12.4573

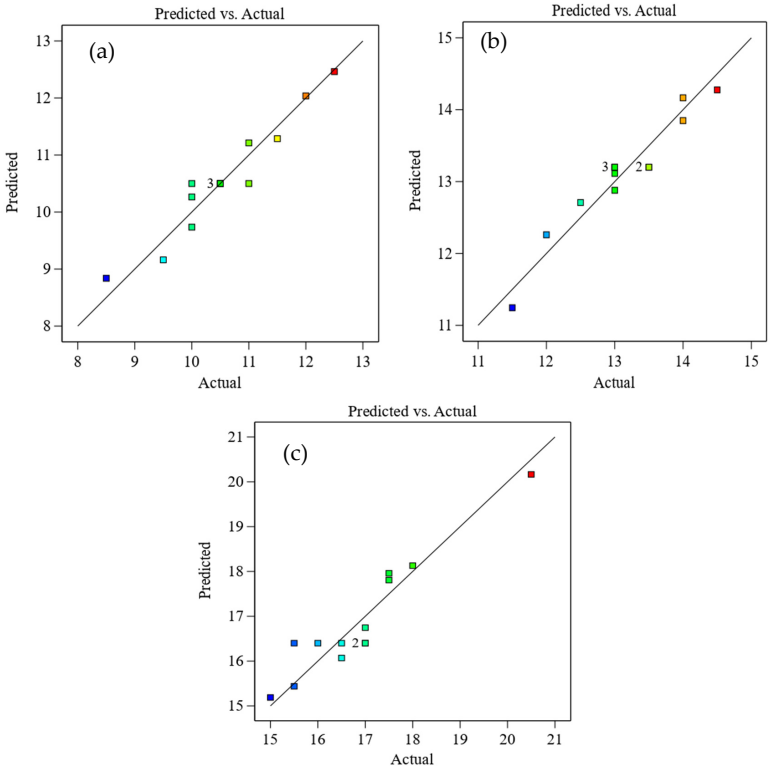

Figure 8. Predicted F_C vs. experimental values at (**a**) 7 days, (**b**) 14 days, and (**c**) 28 days ages.

The influence of LS and CCW on the concrete compressive strength is diagrammatically presented using 2D and 3D plots, as depicted in Figure 9. The relationship between the input variables is observed using contour and three-dimensional (3D) form. The contour and three-dimensional plots of compressive strength showed a strong correlation between lateritic soil and CCW. The compressive strength response to lateritic soil is comparatively

higher and more positively impacted than CCW's. This outcome matched the findings of the experiment.

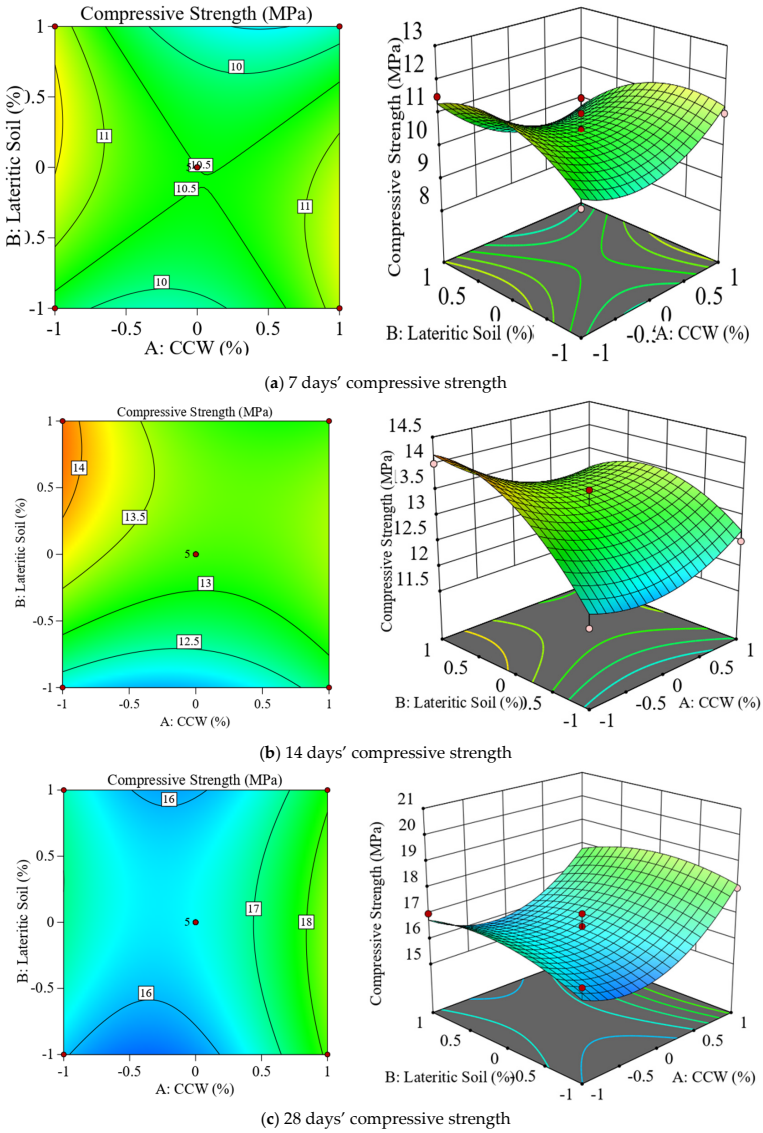

Figure 9. Contour and 3D plots for compressive strength at different ages of curing.

3.3.2. RSM Model for Splitting Tensile Strength

The ANOVA result of the developed model for estimating the laterite concrete splitting tensile strengths is presented in Table 6. Table 6 shows that all model terms were statistically significant, with p-values < 0.05, except model term B for the 7-day splitting tensile strength models and model term B and AB for the 14-day tensile strength. In contrast, 28-day splitting tensile model terms have p-values > 0.05, except term A, which is significant with p-value < 0.05. Therefore, the generated models are denoted as Equations (9)–(11), respectively, for the 7-day, 14-day, and 28-day splitting tensile strength of the concrete, which incorporates lateritic soil and CCW, may be employed for prediction with high precision.

$$F_{S-7} = 0.8022 + 0.1351A - 0.0594B - 0.2768AB + 0.1154A^2 + 0.0719B^2 \quad (9)$$

$$F_{S-14} = 1.11 + 0.3181A + 0.0452B + 0.0324AB + 0.2933A^2 + 0.1947B^2 \quad (10)$$

$$F_{S-28} = 1.86 + 0.3065A + 0.0633B + 0.0006AB + 0.0438A^2 + 0.0575B^2 \quad (11)$$

where $F_{S\text{-}7}$, $F_{S\text{-}14}$ and $F_{S\text{-}28}$ are the 7, 14, and 28-day splitting tensile strengths (MPa), respectively; and A and B denote CCW and LS (%), respectively.

The performance indicators of the developed RSM model for predicting laterite soil concrete splitting tensile strength are summarized in Table 7. The models achieved an R^2 value greater than 90% for both splitting tensile strengths at the three curing ages. The 28-day splitting tensile strength model revealed the highest estimation accuracy with R^2 = 0.9455, followed by R^2 = 0.9409 and 0.9404 for the 7-day and 14-day splitting tensile strength model, respectively. Furthermore, as all of the splitting tensile strength model's discrepancies are less than 0.2, there was a strong agreement between the adjusted and predicted R^2 values. As a result, there should be no issues or significant block impact when using the generated model equations in Equations (9)–(11). The models have a strong predictive capacity with reduced variation between the estimated and experimental findings, as seen by their smaller standard deviations compared to their respective mean values. The scatter plot between the predicted and observed values of splitting tensile strength at the different curing ages is depicted in Figure 10.

Figure 11 shows the 2D and 3D plot describing the correlation between the input variables (LS and CCW) and the splitting tensile strengths. The tensile strength dropped at 7, 14, and 28 days as the proportion of lateritic soil addition increased. These statistical findings are consistent with the test results' outcomes.

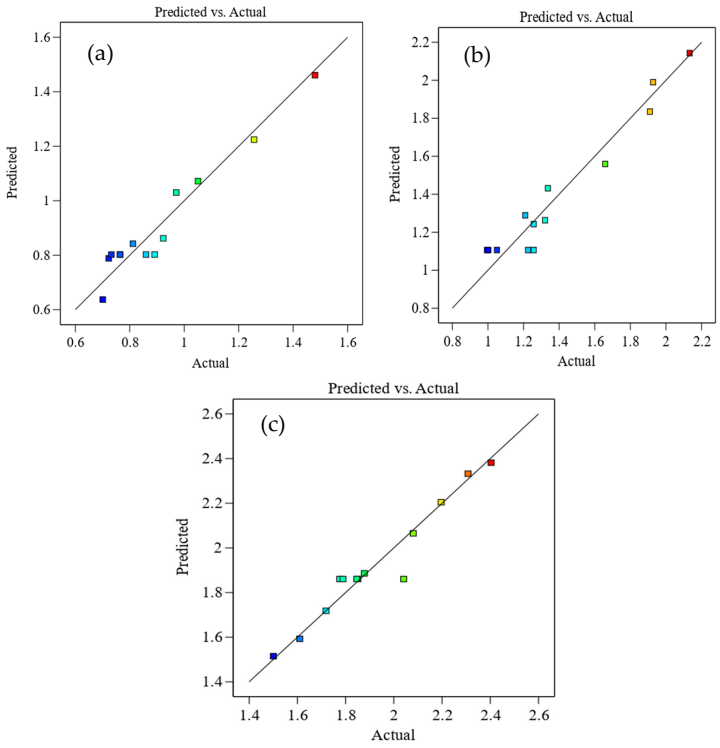

Figure 10. Predicted F_s vs. experimental values at ages of: (**a**) 7 days, (**b**) 14 days, and (**c**) 28 days.

Table 6. ANOVA results for splitting tensile strength models.

Response	Source	Sum of Squares	Mean Square	F-Value	*p*-Value	Significance
F_{S-7} (MPa)	Model	0.5962	0.1192	22.28	0.0004	significant
	A-CCW	0.1459	0.1459	27.27	0.0012	
	B-LS	0.0283	0.0283	5.28	0.0551	
	AB	0.3065	0.3065	57.27	0.0001	
	A^2	0.0927	0.0927	17.32	0.0042	
	B^2	0.0359	0.0359	6.71	0.0359	
	Lack of Fit	0.0184	0.0061	1.29	0.3914	insignificant

Table 6. *Cont.*

Response	Source	Sum of Squares	Mean Square	F-Value	*p*-Value	Significance
F_{S-14} (MPa)	Model	1.60	0.3204	22.10	0.0004	significant
	A-CCW	0.8097	0.8097	55.84	0.0001	
	B-LS	0.0163	0.0163	1.13	0.3237	
	AB	0.0042	0.0042	0.2889	0.6076	
	A^2	0.5986	0.5986	41.28	0.0004	
	B^2	0.2637	0.2637	18.19	0.0037	
	Lack of Fit	0.0382	0.0127	0.8053	0.5529	insignificant
F_{S-28} (MPa)	Model	0.8159	0.1632	24.28	0.0003	significant
	A-CCW	0.7515	0.7515	111.82	<0.0001	
	B-LS	0.0321	0.0321	4.77	0.0652	
	AB	1.434E-06	1.434E-06	0.0002	0.9888	
	A^2	0.0134	0.0134	1.99	0.2014	
	B^2	0.0230	0.0230	3.42	0.1068	
	Lack of Fit	0.0019	0.0006	0.0571	0.9797	insignificant

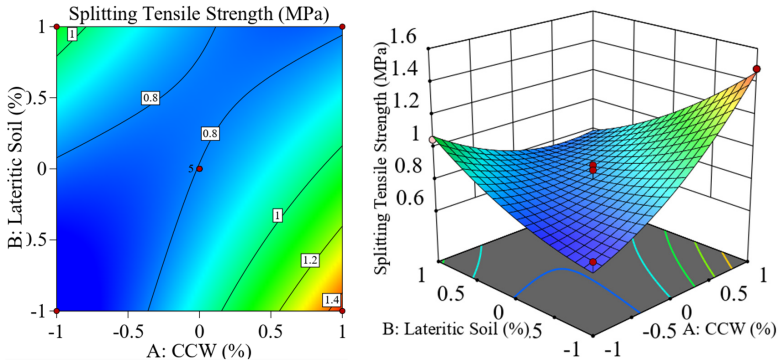

(**a**) 7 days' splitting tensile strength

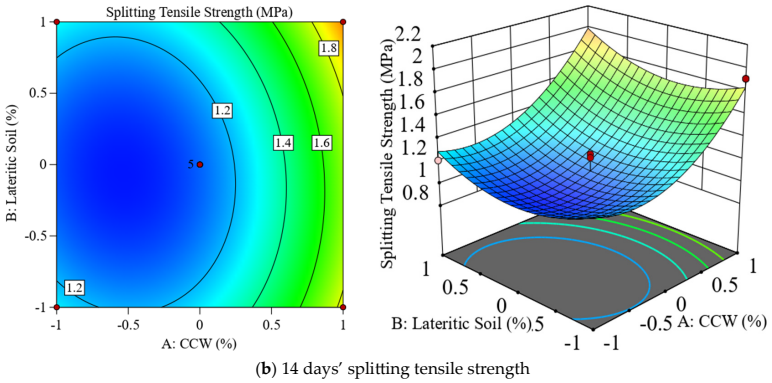

(**b**) 14 days' splitting tensile strength

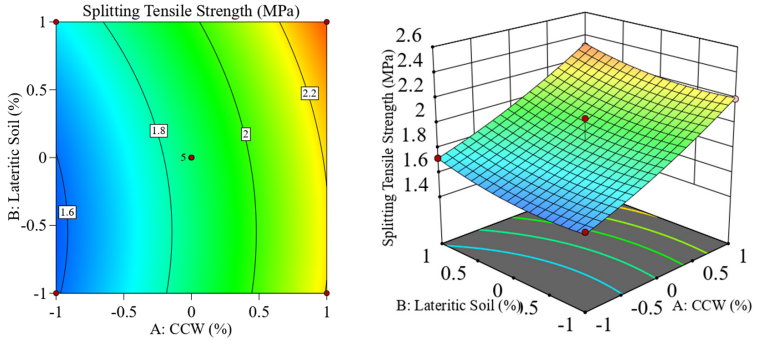

(**c**) 28 days' splitting tensile strength

Figure 11. Contour and 3D plots for splitting tensile strength at different curing ages.

Table 7. Performance indicators for splitting tensile strength models.

Factors	F_{S-7} (MPa)	F_{S-14} (MPa)	F_{S-28} (MPa)
Std Dev	0.0732	0.1204	0.0820
Mean	0.9175	1.41	1.92
CoV.(%)	7.97	8.56	4.26
R^2	0.9409	0.9404	0.9455
Adjusted R^2	0.8986	0.8979	0.9065
Predicted R^2	0.7461	0.7824	0.9024
Adeq Precision	16.5739	12.6716	15.5653

3.4. Diagnostic Plots for Mechanical Properties Models

The diagnostic diagram of the developed model for predicting the mechanical properties is shown in Figures 12 and 13. The observed value strongly agrees with the predicted value, as indicated by the diagnostic plots, showing that the residuals have a normal distribution. The displayed normal plots for each model showed that the plotted data points were strikingly consistent with the straight regular lines. It was thus verified that each model fits neatly into the normal probability distribution. Models 9, 10, and 11, quadratic models for splitting tensile strength, exhibited the highest R^2 values of 0.9409, 0.9404, and 0.9455, respectively, suggesting they possess the most predictive potential. Additionally, the R^2 values of 0.9282, 0.9252, and 0.8973 were attained by the quadratic models for compressive strength (models 6, 7, and 8), demonstrating good predictive potential. The majority of the measured responses were in proximity to the reference standard. This demonstrates unequivocally how excellent the computed quadratic models were in estimating the observed responses. Only the properties of raw materials and the experimental range of mixing parameters are covered by the suggested derived models with sufficient predictions. The best correlation and prediction are found in quadratic structured models for splitting tensile strength, which also have the highest fitness.

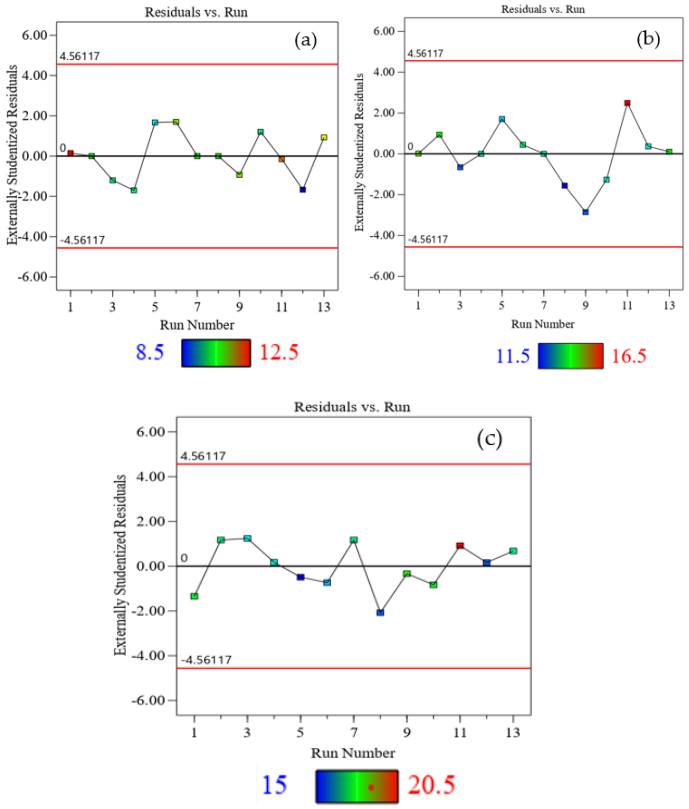

Figure 12. Externally studentized residuals vs. runs plots for: (**a**) F_{c-28}, (**b**) F_{c-28}, (**c**) F_{c-28} (MPa).

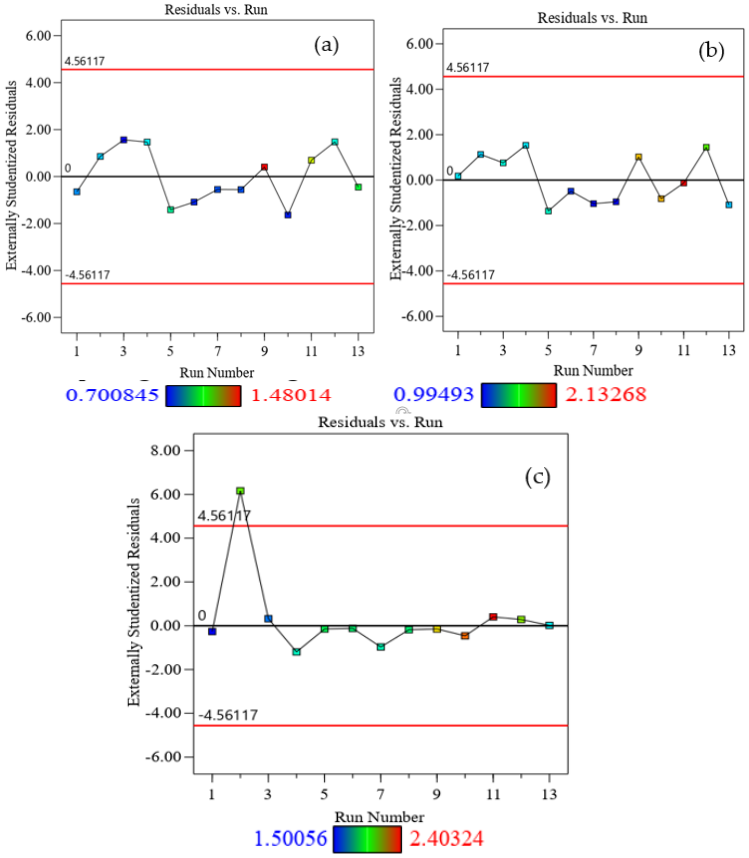

Figure 13. Externally studentized residuals vs. runs plots for: (**a**) $F_{s\text{-}28}$, (**b**) $F_{s\text{-}28}$, (**c**) $F_{s\text{-}28}$ (MPa).

3.5. Optimization

A concrete mix design that will be advantageous for each examined response was achieved by considering all responses simultaneously throughout the optimization operation. When there are several responses, it is critical to identify the acceptable optimum that does not only maximize one, as suggested by Oehlert [49]. While the response was intended to be maximal, the optimization was carried out to obtain the greatest performance of laterite concrete in compressive strength and splitting tensile strength. Range, minimum, maximum, and goal are examples of input optimizations. They are used to establish the parameters that optimize the output value under particular circumstances. The solution variable with the highest desired function value was carefully chosen through optimization. Conversely, advance optimization techniques have been emerged to optimize concrete mixture. For instance, Shigi et al. [50] developed multi objective optimization for evaluating the mixture of recycled aggregate concrete utilizing explainable machine learning algorithms. This optimization technique had yielded a promising result by improving the efficiency of mixture proportion, which resulted a better mechanical and durability-related properties. Similarly, evaluating sustainable concrete based on mixture ratio, static performance and durability were reported using advance artificial intelligent (AI) models in the past literature [51]. Table 8 presents the multi-objective optimization findings. The RSM program selects optimal mixture proportions based on the optimization goals. This involves replacing 10% of the fine aggregate with lateritic soil and using 15% of CCW in cement replacement to achieve the maximum responses and combined desirability of 81.3%. The optimization process's desired outcome is revealed in Figure 14, using the three-dimensional surface graph.

Table 8. Multi-objective criteria and outcomes of optimization.

Variables and Responses	Units	Goal	Lower Limit	Upper Limit	Solution
A: CCW	%	In range	0.00	20.00	15.00
B: LS	%	„	0.00	40.00	10.00
$F_{C\text{-}7}$	MPa	Maximize	8.50	12.50	11.21
$F_{C\text{-}14}$	„	„	11.50	14.50	13.24
$F_{C\text{-}28}$	„	„	15.00	20.50	18.23
$F_{S\text{-}7}$	„	„	0.70	1.48	1.46
$F_{S\text{-}14}$	„	„	0.99	2.13	1.93
$F_{S\text{-}28}$	„	„	1.50	2.40	2.17
Desirability	%	-	-	-	81.3

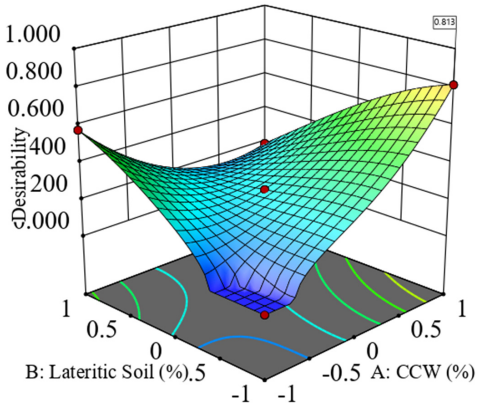

Figure 14. Surface plot for desirability in 3D.

4. Conclusions

The main goal of this investigation was to investigate the effects of lateritic soil and CCW on the mechanical characteristics of concrete. CCW and lateritic soil hybrid integration in concrete was optimized using RSM. The splitting tensile strength and the compressive strength at 7, 14, and 28 days were optimized using six prediction models that were developed. It is feasible to draw the following conclusions:

1. A higher replacement amount of CCW and laterite results in a more workable concrete mix. The remarkable rise in slump might perhaps be ascribed to the particle packing effect of CCW, which decreases the water content needed for plasticization.
2. Regardless of the replacement level, samples produced with CCW and laterite exhibit increasing compressive and splitting tensile strength with age. Nevertheless, it does not appear that the curing medium has a bigger impact on their strength at an early age. The compressive and splitting tensile strength of lateralized concrete has been greatly increased compared to the control sample by incorporating CCW and laterite, up to a 20% substitution of the cement and fine aggregate content.
3. Utilizing RSM, the newly established models were extremely significant in correlation and prediction for the compressive and splitting tensile strength of concrete incorporating lateritic soil and CCW.
4. The best combinations of variables, as determined by the RSM design and analysis, are 15% CCW in place of cement and 10% lateritic soil in substitute of fine aggregate weight. These optimization outcomes produced the most robust possible results, with a desirability of 81.3%.
5. This study indicated that adding CCW to laterite-based concrete significantly improves its mechanical properties. In addition to calcium carbide waste (CCW), other eco-friendly ingredients might be investigated to improve the mechanical properties of laterized concrete. To increase durability and compressive strength, CCW can

be used with other pozzolanic materials like fly ash or silica fume. Investigating further CCW–laterite concrete qualities, especially regarding resilience to fire and acid, requires a future study. Furthermore, long-term research, including lifetime evaluations, should be done on the sustainability and environmental effects of CCW in laterite-based concrete construction. These paths might maximize the qualities of concrete while making a substantial contribution to sustainable building methods.

Author Contributions: A.A.K. and A.M.G.: conceptualization, methodology, investigation, writing—original draft, writing—review, and editing; A.D.R.: writing—original draft, writing—review and editing, and funding acquisition. S.I.H. and Y.E.I.: investigation, visualization, writing—original draft, writing—review and editing. All authors have read and agreed to the published version of the manuscript.

Funding: The authors greatly acknowledge the financial support of this research by the Structures and Materials Laboratory (S&M Lab) of the College of Engineering, Prince Sultan University, Riyadh, Saudi Arabia, for funding the article process fees.

Data Availability Statement: Data are contained within the article.

Conflicts of Interest: The authors declare no conflicts of interest.

References

1. Sun, H.; Li, Z.; Bai, J.; Memon, S.A.; Dong, B.; Fang, Y.; Xu, W.; Xing, F. Properties of Chemically Combusted Calcium Carbide Residue and Its Influence on Cement Properties. *Materials* **2015**, *8*, 638–651. [CrossRef] [PubMed]
2. Raja, R.; Vijayan, P.; Kumar, S. Durability studies on fly-ash based laterized concrete: A cleaner production perspective to supplement laterite scraps and manufactured sand as fine aggregates. *J. Clean. Prod.* **2022**, *366*, 132908. [CrossRef]
3. Aderinola, O.S.; Omolola, O.E.; Quadri, A.I. Effect of Calcium Carbide Waste Powder on Some Engineering Properties of Bamboo Leaf Ash Concrete. *Open Access Libr. J.* **2018**, *5*, 1–15. [CrossRef]
4. Nasiri, S.; Madandoust, R.; Ranjbar, M.M. Investigating the Calcination Temperature and Grinding Time of Calcined Clay on the Mechanical Properties and Durability of LC3 Concrete. *Infrastructures* **2023**, *8*, 139. [CrossRef]
5. Adamu, M.; Ayeni, K.O.; Haruna, S.I.; Ibrahim Mansour, Y.E.-H.; Haruna, S. Durability performance of pervious concrete containing rice husk ash and calcium carbide: A response surface methodology approach. *Case Stud. Constr. Mater.* **2021**, *14*, e00547. [CrossRef]
6. Castano, J.E.; Abdel-Mohti, A. Assessing the Impact of Recycled Concrete Aggregates on the Fresh and Hardened Properties of Self-Consolidating Concrete for Structural Precast Applications. *Infrastructures* **2024**, *9*, 177. [CrossRef]
7. Udoeyo, F.F.; Iron, U.H.; Odim, O.O. Strength performance of laterized concrete. *Constr. Build. Mater.* **2006**, *20*, 1057–1062. [CrossRef]
8. Obi-Egbedi, R.B. Geotechnical Properties of Laterites—A Case Study of Lateritic Soil Deposits at Obigbo, Rivers State. Bachelor's Thesis, Federal University of Technology, Owerri, IM, Nigeria, 1998.
9. Orangun, C.O. Local materials in structural engineering. In Proceedings of the Symposium on Local Materials in Civil Engineering Construction, 1988; Nigeria Society of Engineers: Abuja, Nigeria, 1988; pp. 20–27.
10. Ogunbode, E.B.; Egba, E.I.; Olaiju, O.A.; Johnson, C.N.; Amusuk, D.J.; Dodo, Y.A. Determining the properties of green laterized concrete with fly ash for sustainable solid waste management. *Chem. Eng. Trans.* **2018**, *63*, 649–654. [CrossRef]
11. Ephraim, M.E.; Adoga, E.A.; Rowland-Lato, E.O. Durability and Fire Resistance of Laterite Rock Concrete. *Am. J. Civ. Eng. Archit.* **2016**, *4*, 117–124. [CrossRef]
12. Musbau, K.D.; Kolawole, J.T.; Babafemi, A.J.; Olalusi, O.B. Comparative performance of limestone calcined clay and limestone calcined laterite blended cement concrete. *Clean. Eng. Technol.* **2021**, *4*, 100264. [CrossRef]
13. Ettu, L.O.; Ibearugbulem, O.M.; Ezeh, J.C.; Anya, U.C. The Suitability of Using Laterite as Sole Fine Aggregate in Structural Concrete. *Int. J. Sci. Eng. Res.* **2013**, *4*, 502–507. [CrossRef]
14. Raja, R.; Vijayan, P. Investigations on Mechanical Characteristics and Microstructural Behavior of Laterized High Strength Concrete Mix. *Arab. J. Sci. Eng.* **2021**, *46*, 10901–10916. [CrossRef]
15. Ukpata, J.O.; Ewa, D.E.; Success, N.G.; Alaneme, G.U.; Otu, O.N.; Olaiya, B.C. Effects of aggregate sizes on the performance of laterized concrete. *Sci. Rep.* **2024**, *14*, 448. [CrossRef] [PubMed]
16. Haruna, S.; Adamu, M. Effect of hybridization of calcium carbide waste and rice husk ash on the properties of self-compacting concrete. *J. Ceram. Concr. Sci.* **2020**, *5*, 1–10.
17. Chen, S.; Yuan, H. Characterization and optimization of eco-friendly cementitious materials based on titanium gypsum, fly ash, and calcium carbide residue. *Constr. Build. Mater.* **2022**, *349*, 128635. [CrossRef]
18. Tang, P.; Javadi, A.A.; Vinai, R. Sustainable utilisation of calcium-rich industrial wastes in soil stabilisation: Potential use of calcium carbide residue. *J. Environ. Manag.* **2024**, *357*, 120800. [CrossRef]

19. Rattanashotinunt, C.; Thairit, P.; Tangchirapat, W.; Jaturapitakkul, C. Use of calcium carbide residue and bagasse ash mixtures as a new cementitious material in concrete. *Mater. Des.* **2013**, *46*, 106–111. [CrossRef]
20. Gora, A.M.; Ogork, E.N.; Ibrahim Haruna, S. Effect of Calcium Carbide Wastes as Admixture in Mortar. *Sch. J. Eng. Technol.* **2017**, *5*, 655–660. [CrossRef]
21. Obeng, J.; Andrews, A.; Adom-Asamoah, M.; Adjei, S. Effect of calcium carbide residue on the sulphate resistance of metakaolin-based geopolymer mortars. *Clean. Mater.* **2023**, *7*, 100177. [CrossRef]
22. Khongpermgoson, P.; Abdulmatin, A.; Tangchirapat, W.; Jaturapitakkul, C. Evaluation of compressive strength and resistance of chloride ingress of concrete using a novel binder from ground coal bottom ash and ground calcium carbide residue. *Constr. Build. Mater.* **2019**, *214*, 631–640. [CrossRef]
23. Chaitanya, B.K.; Sivakumar, I.; Madhavi, Y.; Cruze, D.; Venkatesh, C.; Naga Mahesh, Y.; Sri Durga, C.S. Microstructural and Residual Properties of Self-Compacting Concrete Containing Waste Copper Slag as Fine Aggregate Exposed to Ambient and Elevated Temperatures. *Infrastructures* **2024**, *9*, 85. [CrossRef]
24. Guo, W.; Bai, Y.; Xu, Z.; Zhang, J.; Zhao, Q.; Wang, D. Stress-strain behavior of low-carbon concrete activated by soda residue-calcium carbide slag under uniaxial and triaxial compression. *J. Build. Eng.* **2022**, *55*, 104678. [CrossRef]
25. Chen, Y.; Wu, X.; Yin, W.; Tang, S.; Yan, G. Effects of Waste Glass Powder on Rheological and Mechanical Properties of Calcium Carbide Residue Alkali-Activated Composite Cementitious Materials System. *Materials* **2023**, *16*, 3590. [CrossRef] [PubMed]
26. Jaramillo, H.Y.; Gómez Camperos, J.A.; Afanador García, N. Development of a Non-Structural Prefabricated Panel Based on Construction and Demolition Waste for Sustainable Construction. *Infrastructures* **2024**, *9*, 135. [CrossRef]
27. Myers, R.H.; Montgomery, D.C.; Anderson-Cook, C.M. *Response Surface Methodology: Process and Product Optimization Using Designed Experiments*; Wiley Series in Probability and Statistics; Wiley: Hoboken, NJ, USA, 2011; ISBN 9781118210475.
28. Montgomery, D.C. *Design and Analysis of Experiments*; John Wiley & Sons: Hoboken, NJ, USA, 2017; ISBN 1119113474.
29. Sarabia, L.A.; Ortiz, M.C. Response Surface Methodology. In *Comprehensive Chemometrics*; Elsevier: Amsterdam, The Netherlands, 2009; Volume 1, pp. 345–390, ISBN 9780444527011.
30. Kumari, M.; Gupta, S.K. Response surface methodological (RSM) approach for optimizing the removal of trihalomethanes (THMs) and its precursor's by surfactant modified magnetic nanoadsorbents (sMNP)—An endeavor to diminish probable cancer risk. *Sci. Rep.* **2019**, *9*, 18339. [CrossRef]
31. Adamu, M.; Marouf, M.L.; Ibrahim, Y.E.; Ahmed, O.S.; Alanazi, H.; Marouf, A.L. Modeling and optimization of the mechanical properties of date fiber reinforced concrete containing silica fume using response surface methodology. *Case Stud. Constr. Mater.* **2022**, *17*, e01633. [CrossRef]
32. Haruna, S.I.; Zhu, H.; Shao, J. Experimental study, modeling, and reliability analysis of impact resistance of micro steel fiber-reinforced concrete modified with nano silica. *Struct. Concr.* **2022**, *23*, 1659–1674. [CrossRef]
33. Al-kahtani, M.S.M.; Zhu, H.; Haruna, S.I.; Shao, J. Evaluation of mechanical properties of polyurethane-based polymer rubber concrete modified ground glass fiber using response surface methodology. *Arab. J. Sci. Eng.* **2023**, *48*, 4695–4710. [CrossRef]
34. Hai, T.; Chaturvedi, R.; Mostafa, L.; Kh, T.I.; Soliman, N.F.; El-Shafai, W. Designing g-C_3N_4/$ZnCo_2O_4$ nanocoposite as a promising photocatalyst for photodegradation of MB under visible-light excitation: Response surface methodology (RSM) optimization and modeling. *J. Phys. Chem. Solids* **2024**, *185*, 111747. [CrossRef]
35. Siamardi, K. Optimization of fresh and hardened properties of structural light weight self-compacting concrete mix design using response surface methodology. *Constr. Build. Mater.* **2022**, *317*, 125928. [CrossRef]
36. Haque, M.; Ray, S.; Mita, A.F.; Bhattacharjee, S.; Shams, M.J. Bin Prediction and optimization of the fresh and hardened properties of concrete containing rice husk ash and glass fiber using response surface methodology. *Case Stud. Constr. Mater.* **2021**, *14*, e00505. [CrossRef]
37. *ASTM C150-00*; Standard Specification for Portland Cement. ASTM International: West Conshohocken, PA, USA, 2000.
38. *BS 1881-125:2013*; Testing Concrete—Method of Mixing and Sampling Fresh Concrete in the Laboratory. BSI Publication: London, UK, 1986.
39. Teychenné, D.C.; Franklin, R.E.; Erntroy, H.C. *Design of Normal Concrete Mixes*, 2nd ed.; Building Research Establishment (BRE) Ltd.: Watford, UK, 1997.
40. *BS EN 12350-2:2000*; Part 2 Testing Fresh Concrete—Part 2: Slump Test. BSI Publication: London, UK, 2000.
41. *BS EN 12390-3:2019*; Testing Hardened Concrete—Compressive Strength of Test Specimens. BSI Publication: London, UK, 2019.
42. Adamu, M.; Trabanpruek, P.; Jongvivatsakul, P.; Likitlersuang, S.; Iwanami, M. Mechanical performance and optimization of high-volume fly ash concrete containing plastic wastes and graphene nanoplatelets using response surface methodology. *Constr. Build. Mater.* **2021**, *308*, 125085. [CrossRef]
43. Awolusi, T.F.; Oke, O.L.; Akinkurolere, O.O.; Sojobi, A.O. Application of response surface methodology: Predicting and optimizing the properties of concrete containing steel fibre extracted from waste tires with limestone powder as filler. *Case Stud. Constr. Mater.* **2019**, *10*, e00212. [CrossRef]
44. Adamu, M.; Mohammed, B.S.; Shahir Liew, M. Mechanical properties and performance of high volume fly ash roller compacted concrete containing crumb rubber and nano silica. *Constr. Build. Mater.* **2018**, *171*, 521–538. [CrossRef]
45. Mohammed, B.S.; Adamu, M. Mechanical performance of roller compacted concrete pavement containing crumb rubber and nano silica. *Constr. Build. Mater.* **2018**, *159*, 234–251. [CrossRef]

46. Mehta, P.K. High-Performance, High-Volume Fly Ash Concrete for Sustainable Development. In Proceedings of the International Workshop on Sustainable Development and Concrete Technology, Beijing, China, 20–21 May 2004; pp. 3–14.
47. Kelechi, S.E.; Uche, O.A.U.; Adamu, M.; Alanazi, H.; Okokpujie, I.P.; Ibrahim, Y.E.; Obianyo, I.I. Modeling and Optimization of High-Volume Fly Ash Self-Compacting Concrete Containing Crumb Rubber and Calcium Carbide Residue Using Response Surface Methodology. *Arab. J. Sci. Eng.* **2022**, *47*, 13467–13486. [CrossRef]
48. Philips, E.S.; Mutuku, R.N.N.; Mwero, J.N. Palm Kernel Shell as Partial Replacement for Normal Weight Aggregate in Concrete. *Civ. Environ. Res.* **2017**, *9*, 40–47.
49. Oehlert, G.W. *Design and Analysis of Experiments: Response Surface Design*; W. H. Freeman: New York, NY, USA, 2000.
50. Wang, S.; Xia, P.; Gong, F.; Zeng, Q.; Chen, K.; Zhao, Y. Multi objective optimization of recycled aggregate concrete based on explainable machine learning. *J. Clean. Prod.* **2024**, *445*, 141045. [CrossRef]
51. Wang, S.; Xia, P.; Chen, K.; Gong, F.; Wang, H.; Wang, Q.; Zhao, Y.; Jin, W. Prediction and optimization model of sustainable concrete properties using machine learning, deep learning and swarm intelligence: A review. *J. Build. Eng.* **2023**, *80*, 108065. [CrossRef]